On the resolution of S waves for orthorhombic parameters from the wavenumber illumination prospective

Vladimir Kazei[1] & Tariq Alkhalifah[1]

June 23, 2019

King Abdullah University of Science and Technology (KAUST), Thuwal, Saudi Arabia

Summary

Orthorhombic anisotropy is typical of naturally fractured reservoirs. This type of anisotropy is caused by a single system of vertical fractures embedded in a horizontally layered medium. Arbitrary orthorhombic elastic anisotropy can be characterized by ten independent parameters, one of which is density. In the best of circumstances, only six of these parameters can be reliably inverted from the P-wave scattered energy. Thus, we access the resolution of S-wave inversion from the wavenumber illumination perspective and show that S waves can resolve the remaining orthorhombic parameters.

Topics

Seismic Anisotropy in Fractured Reservoirs, Seismic Imaging - Theory, Full Waveform Seismic Inversion

Main objective

Investigate spatial resolution for the orthorhombic inversion of S waves.

New aspects

The null-space of the orthorhombic inversion of S waves is derived analytically. The concept of the effective illumination angle is applied to understand the number of recoverable parameters.

Introduction

The subsurface of the earth is generally dominated by horizontally layered structures. Hydrocarbon reservoirs are pre-stressed in the vertical direction, which makes them more prone to fractures in the vertical direction (Fig. 1(a)). Therefore, at the scale of seismic exploration wavelengths, most naturally fractured reservoirs are orthorhombic (Schoenberg and Helbig, 1997). Traditionally, P waves are the primary source of information for seismic exploration. Unfortunately, neither the travel times of P waves (Tsvankin, 1997) nor their amplitudes (Kazei and Alkhalifah, 2018) reveal the full set of orthorhombic parameters. In full-waveform inversion, not all of the elastic orthorhombic parameters seem to be recoverable from P waves (Köhn et al., 2015).

On the other hand, S waves have shorter wavelengths than P waves and, hence, can provide higher resolution in seismic imaging. They have not been widely used in the past in seismic exploration for several reasons. First, they are not excited by explosive sources. However, modern land surveys are acquired with vibrators that excite SV waves and, though they are harder to excite than P waves, SH waves can also be excited and utilized. Also, P waves arrive at the receivers first; therefore, from a processing point of view, they are easier to separate and utilize in inversions based on travel time. Finally, the kinematics of S waves in anisotropic media are rather complicated and, hence, it is difficult to use them in kinematic inversions. However, these disadvantages disappear when full-waveform inversion is applied to characterize the reservoir as it uses full wavefields. The first questions that arise when setting up a multiparameter full-waveform inversion are how many and which parameters can be inverted. Here, we extend the scattering radiation pattern analysis in the wavenumber domain (Devaney, 1984; Mora, 1989; Kazei et al., 2013; Podgornova et al., 2018; Kazei and Alkhalifah, 2018, 2019) to the inversion of S waves.

Theory

The Born approximation for the scattered wavefield $\delta\mathbf{U}$ from a source located at $\mathbf{x}_s$ and a receiver at $\mathbf{x}_g$ for a perturbation in density $\delta\rho(\mathbf{x})$ and the stiffness tensor $\delta c_{ijkl}(\mathbf{x})$ can be expressed as follows (Hudson and Heritage, 1981):

$$\delta\mathbf{U}(\mathbf{x}_s,\mathbf{x}_\mathbf{g},\omega)=\int_{-\infty}^{+\infty}\int_{-\infty}^{+\infty}\int_{-\infty}^{+\infty}(\omega^2\delta\rho(\mathbf{x})\mathbf{u}^0\cdot\mathbf{G}-\nabla\mathbf{u}^0:\delta\mathbf{c}(\mathbf{x}):\nabla\mathbf{G}(\mathbf{x}_g,\mathbf{x}))\mathrm{d}\mathbf{x}, \tag{1}$$

where $\mathbf{u}^0$ is the incident wavefield, $\mathbf{G}$ is the Green's tensor, and ω is the angular frequency. The far-field plane wave approximation of the Green's tensor in equation (1), consisting of P, SV, and SH waves (Snieder, 2002; Podgornova et al., 2018), is used for our further analysis. Different components of the Green's function are approximated locally by plane waves as follows:

$$\mathbf{G}=\mathbf{G}_P+\mathbf{G}_{SV}+\mathbf{G}_{SH},\ \mathbf{G}_P\propto e^{i\frac{\omega}{v_p}\mathbf{g}\cdot(\mathbf{x}-\mathbf{x}_g)}\mathbf{g}\mathbf{g},\ \mathbf{g}=\frac{\mathbf{x}-\mathbf{x}_g}{|\mathbf{x}-\mathbf{x}_g|},(\mathbf{g}\mathbf{g})_{ik}\equiv g_ig_k, \tag{2}$$

The first component, $\mathbf{G}_P$, is approximated by a local plane P wave. The second component represents a shear (S) wave polarized in the vertical plane containing both source and receiver directions. Finally, the third component of the Green's tensor is the SH wave, which is polarized along $\mathbf{g}_\varphi$, which is the horizontal component of S waves.

$$\mathbf{G}_{SV}\propto e^{i\frac{\omega}{v_s}\mathbf{g}\cdot(\mathbf{x}-\mathbf{x}_g)}\mathbf{g}_\theta\mathbf{g}_\theta,\ \mathbf{g}_\theta=\left(\frac{\mathbf{g}\times\mathbf{e}_z}{|\mathbf{g}\times\mathbf{e}_z|}\times\mathbf{e}_z\right),\ \mathbf{G}_{SH}\propto e^{i\frac{\omega}{v_s}\mathbf{g}\cdot(\mathbf{x}-\mathbf{x}_g)}\mathbf{g}_\varphi\mathbf{g}_\varphi,\mathbf{g}_\varphi=\left(\frac{\mathbf{g}\times\mathbf{e}_z}{|\mathbf{g}\times\mathbf{e}_z|}\right). \tag{3}$$

SV − SH scattering

The amplitude of the scattered SV-SH wave is proportional to a linear combination of the Fourier transforms of the perturbed parameters, analogous to the case of P-waves (Kazei and Alkhalifah, 2018):

$$\delta U_{SVSH}(\mathbf{s},\mathbf{g},\omega)\equiv\int_V e^{i\mathbf{K}_{SS}\cdot\mathbf{x}}(\mathbf{s}_\theta\cdot\mathbf{g}_\varphi\delta\rho+\mathbf{s}\mathbf{s}_\theta:\delta\mathbf{c}:\mathbf{g}\mathbf{g}_\varphi)\mathrm{d}\mathbf{x}=\mathbf{s}_\theta\cdot\mathbf{g}_\varphi\delta\hat{\rho}(\mathbf{K}_{SS})+\mathbf{s}\mathbf{s}_\theta:\delta\hat{\mathbf{c}}(\mathbf{K}_{SS}):\mathbf{g}\mathbf{g}_\varphi, \tag{4}$$

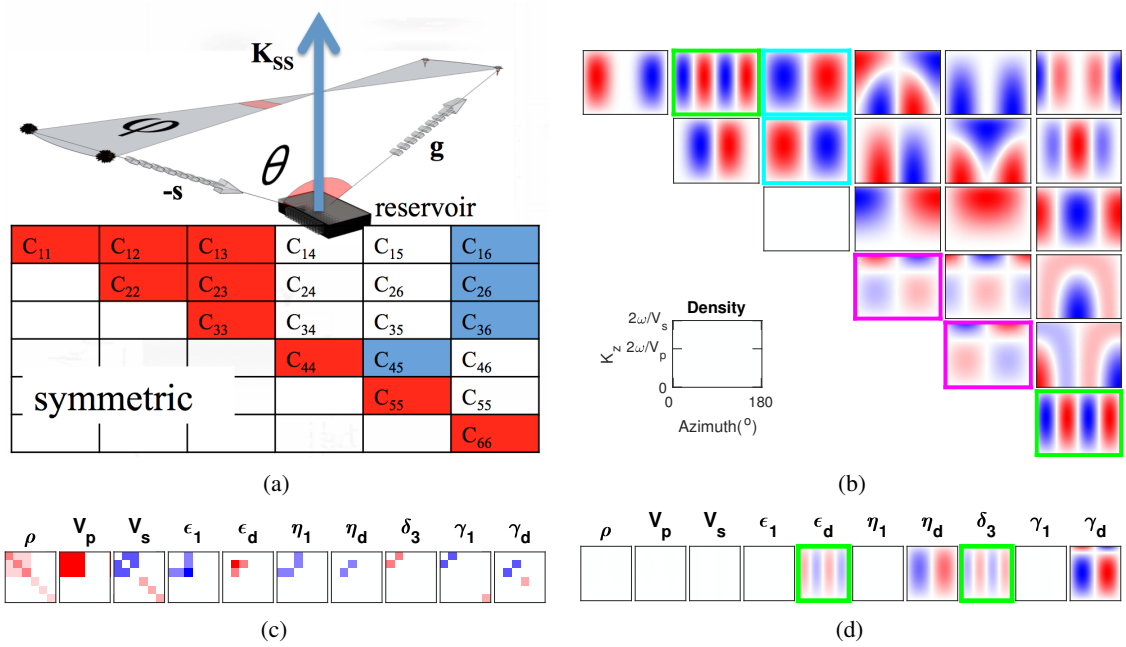

Figure 1 *(a) Elements of stiffness matrix in Voigt notation. Orthorhombic media can be represented by elements in red cells, monoclinic with horizontal symmetry plane by red and blue cells. (b) Spectral sensitivities to vertical wavenumbers for $SV-SH$ scattering in C_{ij},ρ parameterization. Sensitivity to all but C_{33} and density parameters is non zero if we start from isotropic background. Elements establishing similar scattering have the same color frames. Poisson ratio is assumed to be 0.25 ($V_p/V_s=\sqrt{3}$). (c) Partial derivatives of parameters in the h-parametrization w.r.t. the C_{ij} parameters. (d) Same as (b) but for h-parameterization. All VTI parameters don't scatter in this mode; δ_3 and ε_d show similar scattering.*

where the $\mathbf{s}$ and $\mathbf{g}$ vectors point towards the source and receiver, respectively, and $\mathbf{K}_{SS}=\frac{\omega}{V_s}(\mathbf{s}+\mathbf{g})$ (Fig. 1(a)). For the case of a point scatterer $\delta\hat{\rho}(\mathbf{K})=const,\delta\hat{c}_{ijkl}(\mathbf{K})=const$, equation (4) provides the radiation pattern, or scattering function, of these scatterers (Eaton and Stewart, 1994; De Hoop et al., 1999; Shaw and Sen, 2004). Similarly to P-P scattering (Kazei and Alkhalifah, 2018), we focus on the vertical wavenumbers in the perturbation, which lead to the following relations (the vertical axis is labeled x_3, while the azimuth, φ, is measured from the x_1 axis):

$$\delta U_{SVSH}(k_z,\varphi,\omega(k_z,K_z))\propto\mathbf{A}^T_{SVSH}(k_z,\varphi)(\delta\rho(K_z),\delta\mathbf{c}(K_z))^T,\ \ or\ \ \delta\mathbf{U}_{SVSH}(K_z)\propto\mathbb{A}_{SVSH}\delta\mathbf{m}(K_z). \quad (5)$$

Vector $\mathbf{A}(k_z,\varphi)$ is essentially a set of reflection-based radiation patterns remapped into the normalized wavenumber domain (Fig. 1(b)). Some tradeoff is revealed in Fig. 1(b), yet more can be revealed using a hierarchical parameterization (Oh and Alkhalifah (2016); Kazei and Alkhalifah (2018), h-parametrization). The h-parameterization divides the ten parameters required to describe the orthorhombic model into three groups: V_p,V_s, and ρ characterize the isotropic part of the medium, the Alkhalifah-Tsvankin parameters (Alkhalifah and Tsvankin, 1995) $\varepsilon_1,\eta_1,\gamma_1$ complete the general vertical transversally isotropic (VTI) part, and $\varepsilon_d,\eta_d,\gamma_d,\delta_3$ describe the azimuthal variation of the VTI medium (setting these to zero renders the medium VTI). Radiation patterns for the hierarchical parameterization follow from the chain rule.

The SV-SH scattering cannot happen in VTI media since there is no preferred direction for the scattered SH-wave polarization. This type of scattering, if it happens, is a clear indicator of azimuthal anisotropy. This is reflected in the sensitivity diagrams in Fig. 1(d) in which only the orthorhombic parameters in the h-parametrization exert such scattering. An additional tradeoff in this case is the coupling of ε_d and δ_3 (Fig. 1(d)). We derive the exact relation between the patterns of ε_d and δ_3 below:

$$\begin{aligned}\mathscr{R}_{SV-SH,\varepsilon_d}=\mathscr{R}_{SV-SH,2\mathbf{C}_{22}+\mathbf{C}_{23}}&=s_2s_{\theta 2}g_2g_{\varphi 2}+s_2s_{\theta 2}g_3g_{\varphi 3}+s_3s_{\theta 3}g_2g_{\varphi 2}=\\ &s_2s_{\theta 2}g_2g_{\varphi 2}+s_3s_{\theta 3}g_2g_{\varphi 2}=(s_2s_{\theta 2}+s_3s_{\theta 3})g_2g_{\varphi 2}=\\ (\mathbf{s}\cdot\mathbf{s}_\theta-s_1s_{\theta 1})g_2g_{\varphi 2}=-s_1s_{\theta 1}g_2g_{\varphi 2}&=-\frac{1}{2}\mathscr{R}_{SV-SH,2\mathbf{C}_{12}}=-\frac{1}{2}\mathscr{R}_{SV-SH,\delta_3}.\end{aligned} \quad (6)$$

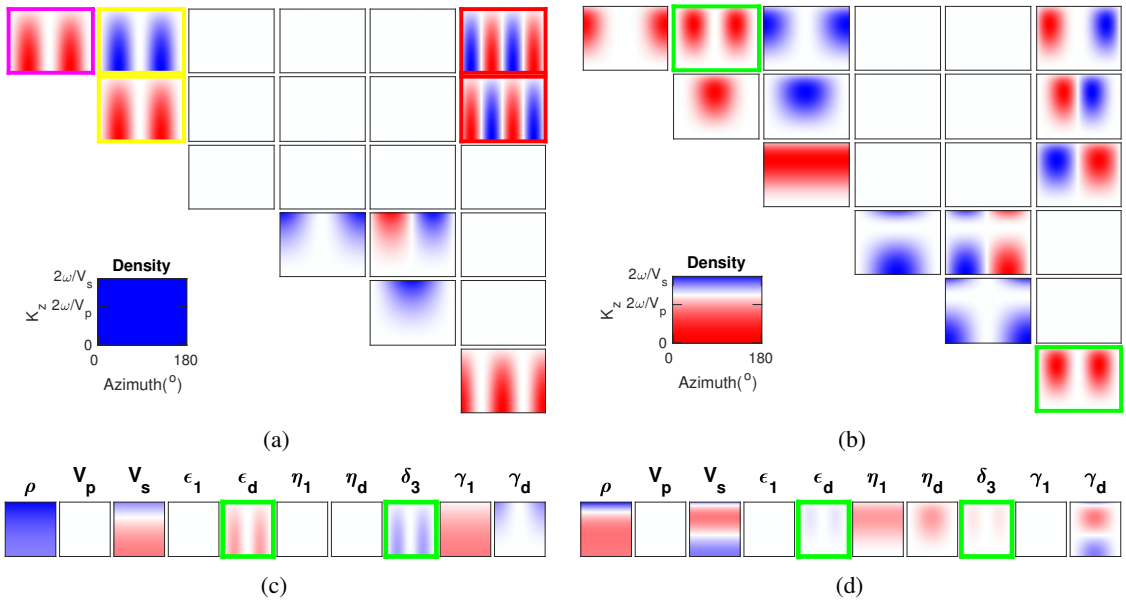

Figure 2 *(a) and (b) Same as Fig. 1(b), but for $SH-SH$, and $SV-SV$ scattering. (c) and (d) Same as Fig. 1(d) , but for $SH-SH$, and $SV-SV$ scattering, respectively*

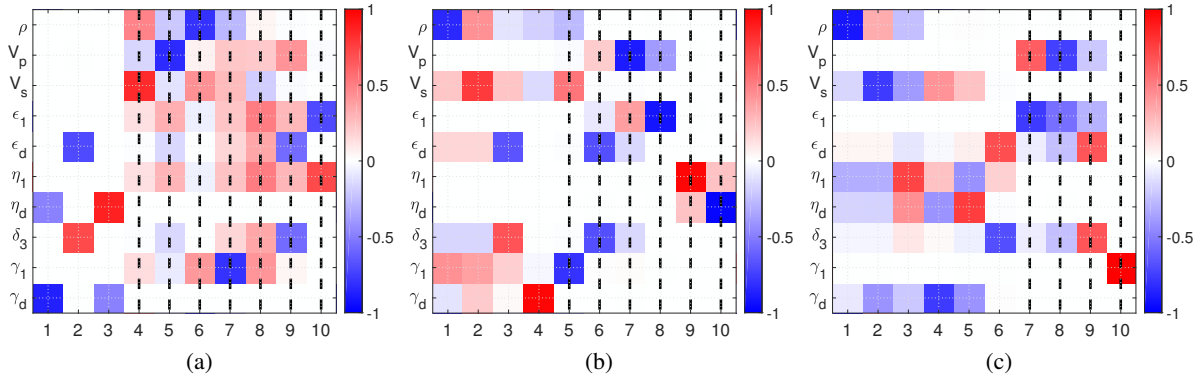

Figure 3 *Singular vectors for the h-parametrization and (a) SV-SH, (b) SH-SH, (c) SV-SV scattering*

$SH-SH$ and $SV-SV$ scattering

The scattering of SH waves in the wavenumber domain is governed by the equation

$$\delta U_{SHSH} \equiv \mathbf{s}_\varphi \cdot \mathbf{g}_\varphi \delta\hat{\rho}(\mathbf{K}_{SS}) + \mathbf{ss}_\varphi : \delta\hat{\mathbf{c}}(\mathbf{K}_{SS}) : \mathbf{gg}_\varphi;\ \delta U_{SVSV} \equiv \mathbf{s}_\theta \cdot \mathbf{g}_\varphi \delta\hat{\rho}(\mathbf{K}_{SS}) + \mathbf{ss}_\varphi : \delta\hat{\mathbf{c}}(\mathbf{K}_{SS}) : \mathbf{gg}_\varphi. \quad (7)$$

The polarization of SH waves is horizontal. Therefore, $\mathbf{s}_{\varphi 3} = \mathbf{g}_{\varphi 3} = 0$, which leads to zero sensitivity of the SH scattering to the C_{13}, C_{23}, and C_{33} parameters (Fig. 2(a)). Also, ε_1, η_1, and η_d span the same linear space as the C_{13}, C_{23}, and C_{33} parameters, and all show zero sensitivity (Fig. 2(c)). The central parameter of the SH-wave inversions is the horizontal shear velocity (V_s in the new parameterization), with γ_1 being responsible for the anisotropy between the vertical and horizontal wave propagation. However, the scattering panels Fig. 2(c) show that V_s is strongly coupled with density in a dynamic inversion. Neither V_p nor the equivalent λ perturbation of the parameters scatter SH waves (Wu and Aki, 1985). Density shows a constant scattering amplitude according to equation (7), which is coupled to a combination of C_{11}, C_{44}, C_{55}, and C_{66}. There exists a non-scattering perturbation $\boldsymbol{\rho} - 2\mathbf{C}_{12} + \mathbf{C}_{66} - \mathbf{C}_{44} - \mathbf{C}_{55}$, which is equivalent to $2\varkappa\boldsymbol{\rho} - (1+\varkappa)\mathbf{V}_s + 2\boldsymbol{\gamma}_1$, according to the partial derivative matrix $\frac{\partial \mathbf{C}}{\partial \mathbf{m}}$ (Fig. 1(c)).

Just like P waves, SV-SV waves are only sensitive to monoclinic parameters (Fig. 2(b)). In the h-parameterization, V_p, γ_1, and ε_1 do not scatter these types of waves. Scattering by density (ρ) resembles V_s, and scattering by anomalies in ε_d resemble δ_3. There are six non-zero singular values in this case (Fig. 3(c)); therefore, only six parameters can be inverted from the SV-SV scattered waves. Density is

not completely coupled to some parameters and can be recovered, as it is not present in the set of zero singular vectors that span the null-space of inversion. In the h-parameterization, the density strongly resembles V_s. Since $\mathscr{R}_{SV-SV,\delta_3} = -\mathscr{R}_{SV-SV,\varepsilon_d}$, the sum of ε_d and δ_3 does not scatter in the reflection mode $\mathscr{R}_{SV-SV,\varepsilon_d+\delta_3} \equiv 0$, which can be showed analytically, similar to (6).

Discussion and conclusions

We evaluated and analyzed the scattering in the wavenumber domain for both S waves, using orthorhombic scatterers visually, and with SVD. SV-SH scattering does not happen in VTI media. Thus, it is a clear indicator of azimuthal anisotropy and can lead to the recovery of three azimuthally anisotropic parameters in orthorhombic media. Namely, γ_d and η_d parameters could be inverted from this type of wave. SV-SV scattering is sensitive to six orthorhombic parameters. SH-SH scattering is sensitive to four parameters and is needed to resolve the γ_1 parameter. The ε_d and δ_3 parameters cannot be decoupled using only scattered S waves.

Acknowledgments

We thank King Abdullah University of Science and Technology (KAUST) for support.

References

Alkhalifah, T. and Tsvankin, I. [1995] Velocity Analysis for Transversely Isotropic Media. *Geophysics*, **60**(5), 1550–1566.

De Hoop, M.V., Spencer, C. and Burridge, R. [1999] The Resolving Power of Seismic Amplitude Data: An Anisotropic Inversion/Migration Approach. *Geophysics*, **64**(3), 852–873.

Devaney, A.J. [1984] Geophysical Diffraction Tomography. *IEEE Transactions on Geoscience and Remote Sensing*, **GE-22**(1), 3–13.

Eaton, D.W.S. and Stewart, R.R. [1994] Migration/Inversion for Transversely Isotropic Elastic Media. *Geophysical Journal International*, **119**(2), 667–683.

Hudson, J. and Heritage, J. [1981] The Use of the Born Approximation in Seismic Scattering Problems. *Geophysical Journal International*, **66**(1), 221–240.

Kazei, V. and Alkhalifah, T. [2018] Waveform Inversion for Orthorhombic Anisotropy with P-Waves: Feasibility & Resolution. *Geophysical Journal International*, ggy034.

Kazei, V. and Alkhalifah, T. [2019] Scattering Radiation Pattern Atlas: What Anisotropic Elastic Properties Can Body Waves Resolve? *JGR Solid Earth (submitted)*.

Kazei, V., Troyan, V., Kashtan, B. and Mulder, W. [2013] On the Role of Reflections, Refractions and Diving Waves in Full-Waveform Inversion. *Geophysical Prospecting*, **61**(6), 1252–1263.

Köhn, D., Hellwig, O., De Nil, D. and Rabbel, W. [2015] Waveform Inversion in Triclinic Anisotropic Media—a Resolution Study. *Geophysical Journal International*, **201**(3), 1642–1656.

Mora, P. [1989] Inversion = Migration + Tomography. *Geophysics*, **54**(12), 1575–1586.

Oh, J.W. and Alkhalifah, T. [2016] Elastic Orthorhombic Anisotropic Parameter Inversion: An Analysis of Parameterization. *GEOPHYSICS*, **81**(6), C279–C293.

Podgornova, O., Leaney, S. and Liang, L. [2018] Resolution of VTI Anisotropy with Elastic Full-Waveform Inversion: Theory and Basic Numerical Examples. *Geophysical Journal International*, ggy116–ggy116.

Schoenberg, M. and Helbig, K. [1997] Orthorhombic Media: Modeling Elastic Wave Behavior in a Vertically Fractured Earth. *GEOPHYSICS*, **62**(6), 1954–1974.

Shaw, R.K. and Sen, M.K. [2004] Born Integral, Stationary Phase and Linearized Reflection Coefficients in Weak Anisotropic Media. *Geophysical Journal International*, **158**(1), 225–238.

Snieder, R. [2002] Chapter 1.7.1 - General Theory of Elastic Wave Scattering. In: Pike, R. and Sabatier, P. (Eds.) *Scattering*, Academic Press, London, 528–542.

Tsvankin, I. [1997] Anisotropic Parameters and P-Wave Velocity for Orthorhombic Media. *Geophysics*, **62**(4), 1292–1309.

Wu, R.S. and Aki, K. [1985] Scattering Characteristics of Elastic Waves by an Elastic Heterogeneity. *Geophysics*, **50**(4), 582–595.